Signal Analysis for Failure Detection

M.C. Parpaglione*, L.V. Pérez†, D.A. Rubio*,
D. Czibener*, C.E. D'Attellis*, P.I. Brudny*
and J.E. Ruzzante‡
Comisión Nacional de Energía Atómica.
Av. del Libertador 8250 (1429) Buenos Aires, Argentina.
E-mail: parpagli@cnea.edu.ar

Abstract

Several methods for analysis of acoustic emission signals are presented. They are mainly oriented to detection of changes in noisy signals and characterization of higher amplitud discrete pulses or bursts. The aim was to relate changes and events with failure, crack or wear in materials, being the final goal to obtain automatic means of detecting such changes and/or events. Performance evaluation was made using both simulated and laboratory test signals.

The methods being presented are the following:

1. Application of the Hopfield Neural Network (NN) model for classifying faults in pipes and detecting wear of a bearing.
2. Application of the Kohonnen and Back Propagation Neural Network model for the same problem.
3. Application of Kalman filtering to determine time ocurrence of bursts.
4. Application of a bank of Kalman filters (KF) for failure detection in pipes.
5. Study of amplitude distribution of signals for detecting changes in their shape.
6. Application of the entropy distance to measure differences between signals.

This work is partially supported by IAEA Research Contract Number 5987/R1/RB.

Introduction

We analyzed acoustic emission signals (AES). They are the electric response of a piezoelectric transducer to an excitation consisting of elastic waves. Elastic waves are emitted by a material during development of plastic deformation or development and crack growth. AES can be seen as a series of decaying bursts, stochastically spaced and with random amplitudes. When monitoring the transducer output, each burst results in the form of decaying oscillations within frequencies 50 KHz to 1MHz.(Fig 2). We may distinguish two kinds of AES: low amplitude continuous emission and higher

*Centro de Cálculo Científico
†Consejo Nacional de Investigaciones Científicas y Técnicas
‡Departamento de Materiales

amplitude discrete bursts. Random noise is always present. AES had been analyzed by Fourier techniques, Gabor or Wavelet transforms,etc. and also using only bursts parameters, i.e. amplitude, duration and rise-time, whose definition is clear from Fig. 1. The approach presented here uses neural networks, Kalman filtering, usual statistics and time series results.

1 Neural Networks

1.1 General Concepts

Neural Network (NN) computing model is based on actual brain NN. A NN is defined by its architecture and by the activation function it uses (see [1]). Network architecture depends on neurons and synaptic weight matrix. Neurons are simple processing units where a weighted sum of inputs is done. The synaptic matrix contains synaptic junction weights between pairs of neurons. It is respectively possitive or negative according to excitatory or inhibitory synapse. Network training for each determined task consists of *fitting the strenght of synapse*. A different NN models arises from each architecture, as for example: Hopfield model, Back Propagation, Kohonen features mapping, etc. Not all problems can be solved with any model. It will depend on interconnections and activation functions.

1.2 Hopfield Model

This model recovers a given set of images in such a way that if a previously learned fuzzy or noisy image is entered, the network is capable of returning the complete original image.

1.3 Back Propagation

A set of patterns is given as input. Network is trained to obtain the desired output. This is accomplised by minimizing mean square differences between network output and desired output.

Once trained, the network was capable of producing a reasonable answer even for patterns not belonging to the training set (pattern: input problem representation).

1.4 Kohonen feature mapping

It maps input patterns onto an output matrix. Only one neuron of the output matrix gives an answer when the network is excited by each input pattern. The goal was having grouped similar input patterns in neighboring locations of the output matrix. This network preserves input features.

2 Applications of Neural Networks

2.1 Hopfield model

In this approach Hopfield model is used to memorize different stages of wear in a bearing. Each event is parameterized as amplitude, duration and rise-time. Afterwards it is discretized in binary matrices so becoming images capable of being memorized.

This approach was also used to memorize pressure zones when pressuring a pipe that had a defective welding in an extreme. The experiment is descript in [3], and the neural network is in [2]. Same parameterization was used.

2.2 Kohonen plus Back Propagation

When locating the source of an Acoustisc Emission, the model that best suits is Back Propagation. The input is a pattern that represents a signal and the output is a distance. One drawback of this model is that, to avoid loosing signal features, it is necessary a high sampling frecuency during a reasonable long period. The pattern representing the signal includes too many points, the synaptic matrix results extremely large and processing become difficult. It is then seek an input pattern representation including fewer points. It's done by preprocessing input patterns (previously to the Back Propagation Network) through a Kohonen Network. The latter maps signal features in neighbouring regions.

To enter Kohonen network signal is divided in k windows of a fixed size. So, k coordinates in the matrix are obtained and used as input to the Back Propagation network.

3 Estimation of time occurrence and amplitude of bursts using Kalman filters

Fig. 2 shows a laboratory simulated signal consisting in two bursts of the same amplitude located in $t_1 = 350\mu s$ and $t_2 = 500\mu s$. As can be seen two contiguous bursts can be undistinguishable because they are too close, their amplitudes differs too much, they are masked by background noise, etc. Hence it is worth to estimate time of occurrence and amplitude of bursts, and much better if it can be achieved on line. Ours is a model based approach and make use of Kalman filtering theory, issued about 1960.

3.1 Model assumed

We consider the AES $s(t)$ to be of the form (see [4])

$$s(t) = \sum_{i=1}^{\infty} a_i h(t - t_i)$$

where $h(t) = t^b \exp^{-ct} \sin \omega_0 t \qquad for\ t >= 0$
a_i random variables of a known distribution
t_i random impulses, Poisson distributed
ω_0 transducer resonant frequency
b, c a priori estimated parameters

Using this model, $s(t)$ can be represented as the solution of a dynamical system of the form

$$\begin{cases} \dot{X}(t) &= AX(t) + Bu(t) \\ X(t_0) &= 0 \end{cases}$$

where

A, B are coefficient matrices.

u a one-dimensional excitation of the form $u(t) = \sum_{i=1}^{\infty} a_i \delta(t - t_i)$ where δ is the Dirac delta function

$X(t)$ the state vector, being $s(t)$ one of its components.

3.1.1 Kalman filtering

This is an approach that leads to computing algorithms that provide at each time t an estimate $\hat{x}(t)$ of a random process $x(t)$. It is based on measurements related with $x(t)$ obtained previously to time t. The process to be estimated must satisfy an equation of the form:

$$\begin{cases} \dot{X}(t) &= AX(t) + Bu(t) + Gv(t) \\ X(t_0) &= 0 \end{cases} \tag{1}$$

where

X is the state vector

u is a gaussian white noise with zero mean and known variance.

A, B and G are coefficient matrices.

v any known input.

It must be assumed that the initial value $x(t_0)$ is a gaussian random variable with known mean and variance. There must be also available measurements z_k at time t_k for $k = 0, 1, 2, \ldots$ related with the process by an equation of the form

$$z_k = Hx(t_k) + w_k$$

where H is a matrix and w_k is a white gaussian sequence with zero mean and known variance. Under the above conditions it is possible to obtain for each time t_k an estimate $\hat{x}(t_k)$ of $x(t_k)$ that has minimum variance and is linear on the measurements $z_1, \ldots, z_k$. This result is due to Kalman and leads to an algorithm that allows computing on line the estimate $\hat{x}(t_k)$ as soon as the observation z_k is obtained. The main use of this algorithm has been to obtain the actual signal by filtering both the measurement noise w_k and the uncertainties in the model expresssed through the noise input u in the dynamic model. Nevertheless, we went further in the applications.

3.1.2 Application

Two approximations were made in this point. Firstly, we replace the Poisson impulses process u exciting the system by a sum of strongly decaying exponential functions, i. e.:

$$\sum_{i=1}^{\infty} a_i \delta(t - t_i) \approx \sum_{i=1}^{\infty} a_i \exp^{(-\gamma(t-t_i))}$$

γ a large possitive number. This allows including u as another component of the system of differential equations 1 and so using Kalman filtering to estimate it. Secondly, including u in the state vector the resulting system random input is a Poisson process with zero mean and variance $\lambda * \delta(t - t_i)$. It is observed that first and second moments of this process coincide with those of white noise. So, we directly considered the input as if it were white noise. [5]. By monitoring the signal we obtain noisy measurements that can be modelled as

$$z = s(t) + w = Hx(t) + w$$

by letting $H = [\,0\ 0\ \ldots 1\ \ldots 0\,]$. Hence, we only need to the assumptions on initial conditions necessary to use KF theory.

3.1.3 Results

As output of KF fed with signal measurements it is obtained a new signal where it is easier to distinguish two bursts very close, its relative amplitude and, if a long rise-time is present, the actual initiation of bursts. Figures 2 and 3 show the input signal and that provided by the filter.It is possible to distinguish two pulses of same amplitude approximately located in $320-350\mu s$ and $500-550\mu s$. This fact is not clear in the original signal. It is remarked that the output signal is obtained on line, making so possible to relate ocurrence of bursts with deformations or cracks and further on, with distance to the sensor. It also has to be remarked that this method is based on the model assumed. So, one of the remaining questions is the reliability of the model parameters. Even when numerical experiments showed good results independently of parameter accuracy, we continued this work looking for a method to evaluate the parameter c.

4 Banks of Kalman filters

4.1 Estimation of decay time

The parameter $\tau = \frac{1}{c}$ is called decay time of bursts and is related with source-sensor distance. For this reason and for improving model reliability, we extended the above model based approach by using, instead of one, several filters with the purpose of estimating τ. As has been said, KF are used to estimate the time signal. It is then reasonable to expect that if the estimation is good it will not be very far form the measurements. In other words, the series of the so called "residuals" or "innovations"

$$e_k = z_k - \hat{x}(t_k)$$

should have zero mean and small variance. As τ is not known, a finite set of τ values $\tau_1, \tau_2, \cdots, \tau_m$ is proposed. For each τ_i a different model M_i is obtained. On this base, a different KF_i is designed for each model, constituting a bank of m KF that operates simultaneously in parallel on the measurements (Fig. 4). It is then established a criterion to choose the value τ_{i^*} such that the corresponding KF_{i^*} works best. The criterion consists on choosing the minimimun of S_i, a weigthed sum of the residuals e_k^i. of each filter.In other words, the smaller the residuals , the better the estimation. Weights are obtained from probabilistic considerations [6]

4.2 Results

We tested the method on numerically simulated noisy signals [7]. They were obtained by simulating the stochastic model for a particular value of τ and corrupting with noise. Simulated observations were entered a bank of filters designed for that τ value and several others. The minimun S_i was reached by the KF designed for the τ used in the simulation.

Hence, including the bank of KF allows to improve the model used to estimate time of occurrence of bursts as well as get information about source-sensor distance. Both tasks can be done on-line.

We use a sligthly different approach to solve another problem.

4.3 Application to leakage detection

In figure 5 it can be seen a simplified scheme of double pipe heat exchanger.The failure to be detected is any leak in the inner pipe. In normal operating conditions, velocity in each pipe remains invariant.

If a leak in the inner pipe occurs, velocity is modified due to the flow going from one pipe to the other. We considered both pipes divided in sections. Taking as state variables temperatures of the flow at each section of each pipe, we can reach to a model for normal operating conditions of the form 1, where now X is a vector of temperatures of dimension equal to twice the number of sections. Observations available were tremperatures of the outcoming water from the inner pipe, i.e. measurement model resulted

$$z(t_k) = Hx(t_k) + w_k$$

where $H = [0\ 0\ ...\ 0\ 1\ 0\ ...0]$ and w_k the observation noise, (gaussian, white, zero mean, known variance). So, conditions to design a KF are satisfied.

The coefficients in A, B and G depends on flow velocities in each section. When a failure occurs in one section, velocities in that and subsequent sections change proportionally to the leak size and so do coefficients. Hence for each failure hypothesis $\mathcal{H}_i$, different matrices A_i, B_i and G_i will be obtained, each one leading to a different model $\mathcal{M}_i$ and so to a different filter KF_i.

On this scheme , observation are processed through a bank of filters including that designed on the normal operation model and those designed on models corresponding to each size and location of failure. It is reasonable to expect that, at each time, the filter designed on the actual operating model should work best. We used the criterion mentioned in the previous section to choose it. Hence, while system operates on normal conditions. The sum S_N corresponding to the normal model will be minimum. When a failure occurs, another S_{i*} will become minimum. As M_{i*} models one determined size and location of leak, detection and identification of failure are achieved simultaneously and on line. We evaluated this method simulating leaks of several sizes in different sections [8]. Fig. 6 shows S_i values as function of time. It can be seen that the minimum changes after failure occurrence at time $t = 300s$. It has to be remarked that simulated faults cannot be seen in the observations because the effect produced is smaller than measurements standard deviation.

5 Detecting toolwear by AES amplitude distributions

We sought a method to detect changes in the shape of signal waves that could be related with toolwear. Our approach, began considering segments of the digitized signal as statistical populations and establishing their probability density function. In other words we simply divide the range of amplitudes in several intervals, count how many times the amplitud value fall in each interval and build a frequency histogram. Figure 7 show how different wave shapes result in different probability density shapes.

Third and fourth moments of a distribution, i.e. skew and kurtosis are related with density function shape. Skew refers to the symmetry about its mean and kurtosis to its sharpness. Moreover, they can be easily estimated from data. So if pairs of estimated skew and estimated kurtosis are plotted in the $x - y$ plane, similar distribution shapes will result in neighboring locations.

Then, the method proposed consists of firstly determining the region in the plane corresponding to right working. When pairs of estimated skew and kurtosis computed while monitoring the signal fall outside that region, it will mean that a change in the waves happened, indicating begining of wear.

A drawback is that skew and kurtosis are very sensitive to odd values. So we normalized data and assumed they are Beta-distributed. This distribution depends on two parameters a and b, that are mutually independent and completely determines its shape. Depending on a and b, this distribution takes different asymmetries and changes from bell-shaped to U-shaped. Moreover, a and b can be easily estimated using only mean and standard deviation of data. Skew and kurtosis of Beta distribution may in turn be computed from a and b. So we assumed data were Beta distributed and then determined right working regions for pairs (a,b) and skew and kurtosis of Beta distribution [9].

Figures 8, 9 and 10 show plot obtained by monitoring AES from a bearing rolling without lubrication. It can be seen that pairs obtained near the end of the experience and those of the begining lie in different regions.

6 Entropy distance

This is another idea to determine differences between signals that make use of the entropy distance.

A classical approach to analyze time series is fitting to data the so called Autorregresive (AR) models. It consists of assuming that signal satisfies a difference equation of the form

$$\sum_{i=0}^{p} a_i x_{k-i} = \sigma \epsilon_k$$

where x_i are the signal values, ϵ_i are zero mean gaussian random variables, p the selected order and a_i coefficients that have to be estimated from the signal itself, as well as σ^2.

A comparison of the signal monitored with another used as reference will be done. Modelling both two as AR processes of the same order p, it is possible to compute the joint probability density function of the two signals. It will depend on the parameters fitted.

These probability density functions are computed under two different hypothesis $\mathcal{H}_0$:"both signals fit the same model", $\mathcal{H}_1$:"the signals fit different models" Under $\mathcal{H}_0$, parameters of two signals will be the same and the maximum joint likelihood function results

$$L_0 = \frac{1}{(\hat{\sigma_P}^2 2\pi)^N} \exp(-N)$$

where N is the signal length and $\hat{\sigma_P}$ the standard deviation estimated for a joint signal. Under $\mathcal{H}_1$, two set of parameters have to be considered, hence it results

$$L_1 = \frac{1}{(\hat{\sigma_R}\hat{\sigma_T} 2\pi)^N} \exp(-N)$$

where $\hat{\sigma_R}$ and $\hat{\sigma_M}$ are the standard deviations of reference and monitored signals respectively. Then a likelihood ratio is computed and the entropy distance is defined as [10]

$$d = -2 \ln \frac{L_0}{L_1}$$

This is a non-negative number that is null if and only the parameters are equal, i.e. if the fitted models coincide. The entropy distance is a measure of the statistical difference between two signals. The larger the value of d is, the parameters of the two signals are considered to be more different. By comparing monitored signals with those corresponding tc right working, a threshold may be determined beyond that it is considered that wear began.

We applied this method on the data mentioned in the previous section [9]. Figure 11 show distances computed between segments of the signal at the begining (named with "c") and near the end of the experience("marked with f").

References

[1] Hertz J., Krogh A., Palmer R., *Introduction to the theory of neural computaton*, Lecture notes, Vol. I, Santa Fe Institute, Addison-Wesley Publishing Company, 1991.

[2] Parpaglione M. C., "Neural Networks applied to fault detection using Acoustic Emission", *Non-Destructive Testing 92*, Proceedings of the 13th World Conference on Non-Destructive Testing, São Paulo, Brazil, Vol 1, pp 71-75, October 1992. C.Hallai y P.Kulcsar (Eds.). Elsevier. Pub., 1992.

[3] Straus A., López Pumarega I., Giaccheta R., Asta E., Ruzzante J., "Emisión Acústica en un cordón de soldadura durante la prueba hidráulica", 2° Seminario Latinoamericano de Inspección de Equipo IBP.

[4] Mitrakovic D., Grabek I. and Sedmak S., "Simulation of AE signals and signal analysis systems", Ultrasonic, 23, pp 227-232, 1985.

[5] D'Attellis C.E., Pérez L.V., Rubio A.D and Ruzzante J.E., "Parameter estimation in acoustic emission signals", Journal of Acoustic Emission , Vol. 10, No. 3/4, 1991/92, February 1993.

[6] Magill D.T., "Optimal Adaptive Estimation of Sampled Stochastic Processes", IEEE Transactions on Automatic Control, Vol. AC-10, N. 4, 1965

[7] D'Attellis C.E., Pérez L.V., Rubio A.D and Ruzzante J.E., "A bank of Kalman filters for failure detection using acoustic emission signals", *Non-Destructive Testing'92*. Proceedings of the 13th. International Conference, São Paulo, Brazil, Vol. 1, pp 23-33, October 1992. C.Hallai y P.Kulcsar (Eds.), Elsevier Pub., 1992.

[8] D'Attellis C.E., Pérez L.V., Rubio A.D. and Brudny P.I., "Early failure detection using a bank of Kalman filters: a heat exchanger model" *Non-Destructive Testing'92*. Proceedings of the 13th. International Conference, São Paulo, Brazil, Vol. 1, pp 409-413, October 1992. C.Hallai y P.Kulcsar (Eds.), Elsevier Pub., 1992.

[9] Brudny P.I., Pérez L.V., D'Attellis C.E., "Análisis de señales por métodos estadísticos", Anales de la V Reunión de Trabajo en Procesamiento de la Información y Control, Tucumán, Argentina, 1993.

[10] Chen C.H., "On a segmentation algorithm for seismic signal analysis", Geoexploration, 23 (1984/5) pp 35-40.

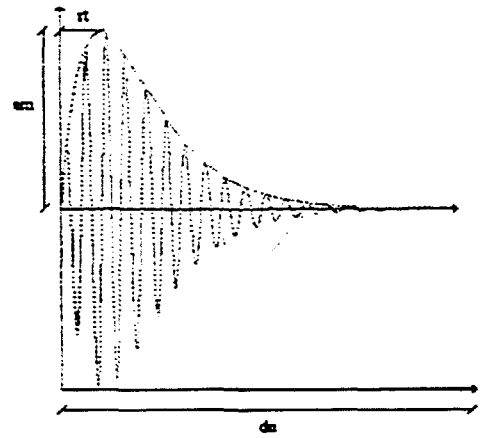

Figura 1: Scheme of a typical Acoustic Emission event

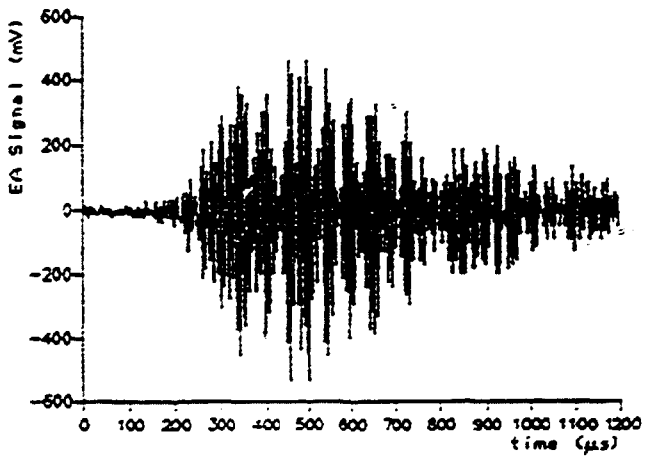

Figura 2: Experimental AE signal

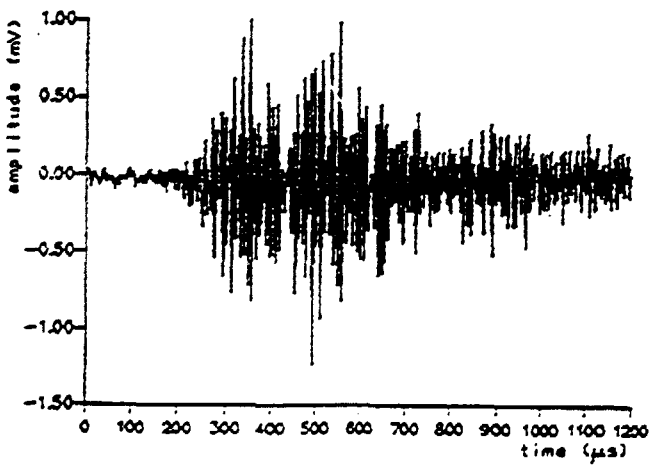

Figura 3: Time occurrence estimation given by Kalman Filter

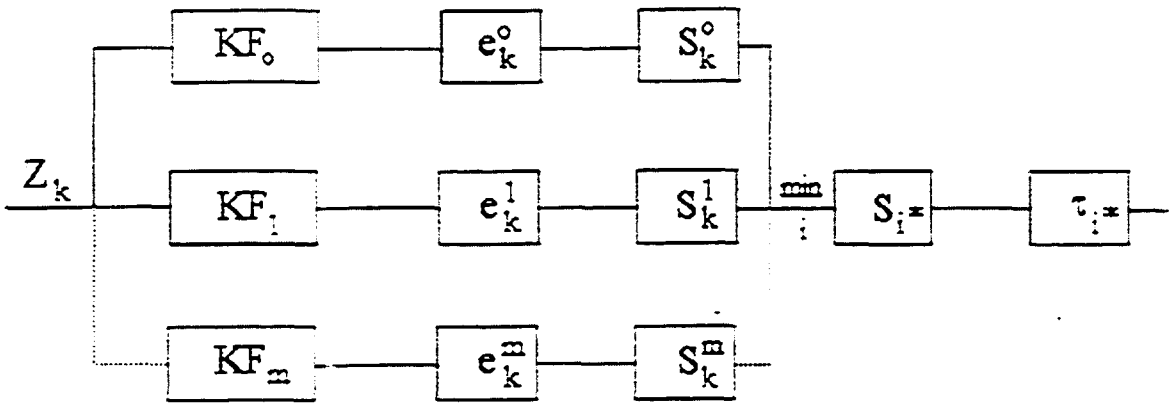

Figure 4: Scheme of the bank of Kalman filters

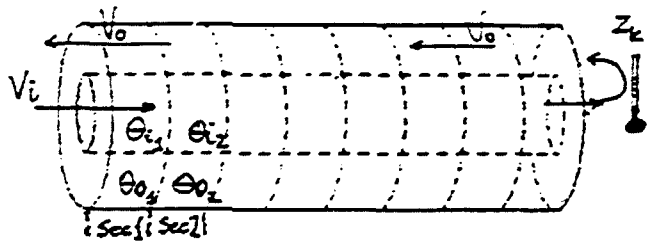

Figure 5: Simplified scheme of a heat exchanger

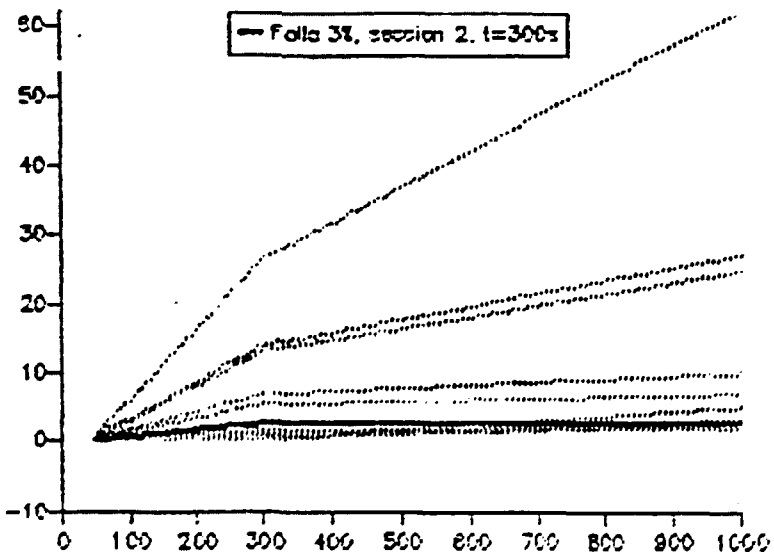

Figure 6: Values of the weigthed sum of innovations to be minimized, corresponds to a failure of 3 percent in second section at $t = 300$

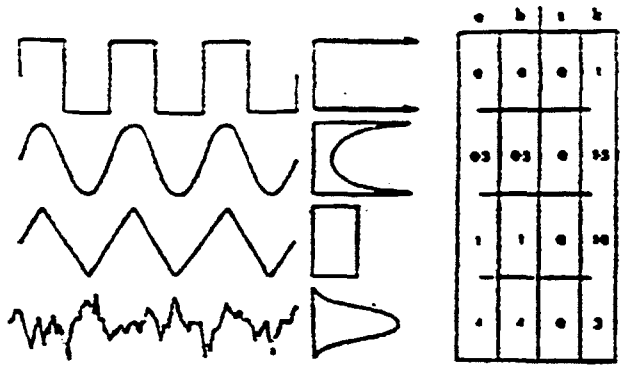

Figure 7: Diferent waves and resulting distribution shapes

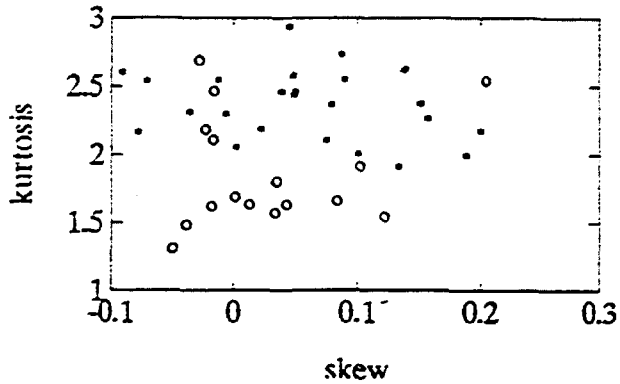

Figure 8: Pairs of skew and kurtosis (o at the begining, $*$ near the end of the experience)

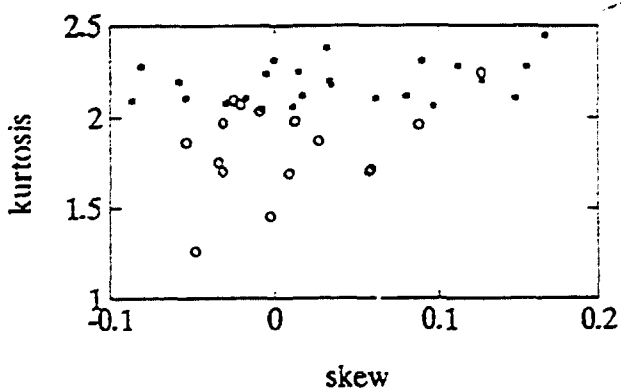

Figure 9: Pairs of skew and kurtosis for β distribution (o at the begining, $*$ near the end of the experience)

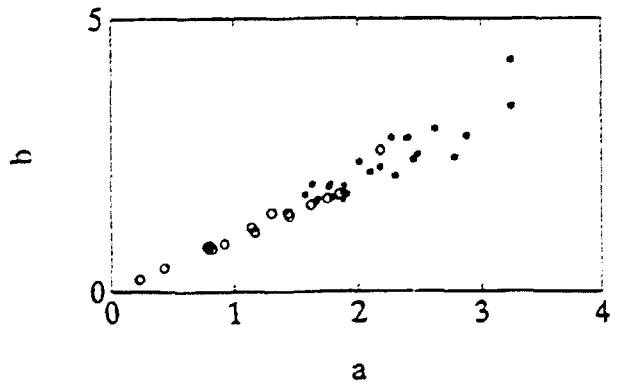

Figure 10: Pairs of parameters a and b of β distribution (o at the begining, $*$ near the end of the experience)

	cb	fa	fb	fc
ca	1034.7	3389.7	2821.6	5671.1
cb	0.0	1253.1	1889.5	3572.7
fa		0.0	1209.1	1563.9
fb			0.0	3297.5

Figura 11: Computed entropy distance (segments *ca* and *cb* corresponds to the begining and the *fa*, *fb* and *fc* corresponds to the end)